NUMERICAL PREDICTION OF FLUID FLOW AND HEAT TRANSFER IN WELDING WITH A MOVING HEAT SOURCE

K. Mundra and T. DebRoy
Department of Materials Science and Engineering, Pennsylvania State University, University Park, Pennsylvania 16802, USA

K. M. Kelkar
Innovative Research, Inc., Minneapolis, MN 55413, USA

An improved computational analysis is presented for the detailed prediction of heat transfer, phase change, and fluid flow during welding with a moving heat source. The governing equations are formulated in a reference frame attached to the heat source. A special feature in the formulation is that the primary unknown velocity is the convective velocity of the fluid with the motion of the heat source, resulting in additional source terms in the equations. The equations are solved using a control-volume-based computational method. The temperature and velocity fields and the time-temperature data are presented for two welding velocities to demonstrate the results using the new technique.

INTRODUCTION

During welding, the interaction of the heat source and the material leads to rapid heating, melting, and vigorous circulation of the molten material in the weld pool. As the heat source moves away from the molten region, solidification of the material takes place. It is now well established that fluid flow and heat transfer are important in determining the size and shape of the weld pool and the weld macrostructures and microstructures [1, 2].

In the past decade, significant progress has been made in the solution of the equations of conservation of mass, momentum, and energy in fusion welding with a stationary heat source [3–5]. However, in practice, the heat source moves with a certain constant velocity. Thus, when viewed in a fixed coordinate system (x, y, z), the welding problem is unsteady. Several investigations of fluid flow and heat transfer in welding using governing equations formulated in this coordinate system have been reported [6, 7]. However, the solution of the equations of conservation of mass, momentum, and energy in this coordinate system requires a large number of grids for accurate representation of the moving, time-dependent position of the heat source and the spatial variation of the heat flux. Furthermore, a small time

Received 4 August 1995; accepted 2 October 1995.

This work was supported by the U.S. Department of Energy, Office of Basic Energy Sciences, Division of Materials Science, under grant DE-FG02-84ER45158 with Pennsylvania State University.

Address correspondence to Dr. K. Mundra, Department of Materials Science and Engineering, Pennsylvania State University, 209 Steidle Building, University Park, PA 16802-5006, USA.

Numerical Heat Transfer, Part A, 29:115–129, 1996

1040–7782/96 $12.00 + .00

NOMENCLATURE

A	function of liquid fraction defined by Eq. (7)	$\mathbf{V}'$	net velocity vector
B	a very small number introduced to avoid division by zero	V_ξ, V_y, V_z	convective velocity components in ξ, y, and z directions
C	a chosen very large positive number	$\mathbf{x}, \xi, y, z$	coordinates
C_p	specific heat	β	thermal expansion coefficient
f_l	fraction of liquid in a cell	ΔH	latent heat content of a cell
F	flow rates through a face of the control volume	γ	surface tension
$F(T)$	latent heat function	$d\gamma/dT$	temperature coefficient of surface tension
g	acceleration due to gravity	η	process efficiency
h	sensible heat	μ	viscosity
H	total heat content	ρ	density
J_h	Gaussian distribution on top surface	τ	Marangoni stress
k	thermal conductivity	$[[p, q]]$	maximum value of p and q
L	latent heat of fusion	**Subscripts**	
P	effective pressure		
Q	laser power	b	bottom face of the control volume
r_b	laser beam radius	B	bottom neighboring point
S_b	buoyancy source term	e	east face of the control volume
$S_{e\text{-}p}$	source term in momentum equations for mushy region	E	east neighboring point
		n	north face of the control volume
S_l	source term in the energy equation	N	north neighboring point
t	time	P	main grid point
T	temperature	s	south face of the control volume
T_l	liquidus temperature	S	south neighboring point
T_{ref}	reference temperature	t	top face of the control volume
T_s	solidus temperature	T	top neighboring point
$\mathbf{U}$	welding velocity vector	w	west face of the control volume
$\mathbf{V}$	convective velocity vector	W	west neighboring point

step is necessary to ensure accuracy and stability of the solution. This makes the computation time very large.

Another approach is to work in the coordinate system that moves with the heat source. In such a case, for a constant welding velocity and a long metal block, the problem becomes steady a short time after the start of welding. Under such conditions, the heat source and the molten metal under the heat source are fixed in space, and the material enters and leaves the computational domain at the welding velocity. This is shown schematically in Figure 1. Kou and Wang [8] solved three-dimensional convection in laser-melted weld pools in the coordinate system attached to the heat source. Prakash et al. [9] proposed a fixed grid numerical methodology to account for phase change during welding and took into account the convection in the weld pool in two dimensions. In the works of Kou and Wang [8] and Prakash et al. [9], the governing equations were solved for the net velocity (combined effect of convective velocity and the material inlet velocity) in the computational domain. The material inlet velocity is taken as equal in magnitude to the welding velocity but opposite in direction.

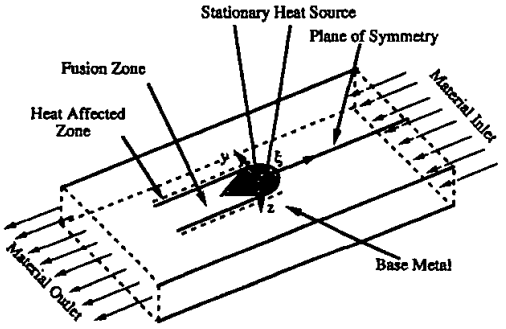

Figure 1. A schematic diagram of the welding process in a coordiante system attached to the heat source.

In the present study, a further modification is incorporated in the governing equations after formulating them in the coordinate system attached to the heat source (ξ, y, z). In the modified formulation, the net velocity in the computational domain is subdivided into the convective velocity and the welding velocity. Furthermore, convective velocity of the fluid is treated as the primary unknown velocity. This results in several simplifications during the computational solution of the governing equations. The convective velocity is zero in the solid region. Therefore the enthalpy-porosity technique [10, 11] can be easily implemented for flow modeling in the mushy zone. Also, the convective velocity is the actual physical velocity of the fluid when viewed in the frame of reference of the stationary block (x, y, z coordinate system). The welding velocity gives rise to physically meaningful source terms in the momentum and energy equations that can be conveniently discretized using the upwind scheme [12]. In this work, the physical situation analyzed corresponds to a three-dimensional laser welding problem. A control volume method described by Patankar [12, 13] has been implemented for the discretization of the governing equations. The SIMPLER algorithm [13] is used for the solution of the discretization equations.

PHYSICAL SITUATION

During laser welding, absorption of energy from the beam results in melting of the solid and formation of the molten pool. A strong temperature gradient exists on the weld pool surface that gives rise to strong Marangoni convection in the molten weld pool. In addition, the temperature differences in the weld pool also give rise to a buoyancy force, which provides an additional driving force for the motion of the liquid. As the heat source moves away from the molten region, the material cools and solidifies.

In this work, laser welding of an alloy using a moving heat source is computationally investigated in three dimensions. The physical situation is schematically shown in Figure 1. Two welding velocities are considered: 0.0027 m/s (high) and 0.0014 m/s (low). The laser power used for both cases is 6000 W. The other process parameters and the thermophysical properties of the material used in

Table 1. Data used for the calculation of temperature and velocity field

Property/parameter	Value
Laser power (W)	6000
Beam radius (m)	2×10^{-3}
Absorption coefficient	0.2
Density (kg/m^3)	7200.0
Solidus temperature (K)	1745.0
Liquidus temperature (K)	1785.0
Viscosity (kg/m s)	3.0×10^{-2}
Thermal conductivity of solid [J/(m s K)]	25.1
Thermal conductivity of liquid [J/m s K]	4.18×10^{2}
Specific heat of solid [J/(kg K)]	702.0
Specific heat of liquid [J/(kg K)]	807.0
Latent heat of melting (J/kg)	2.68×10^{5}
Coefficient of thermal expansion (1/K)	1×10^{-4}
Temperature coefficient of surface tension [N/(m K)]	-3.0×10^{-3}

the computations are presented in Table 1. A temperature difference of 40 K was assumed between the liquidus and solidus temperatures. The energy distribution from the heat source is considered Gaussian in nature.

MATHEMATICAL FORMULATION

Governing Equations

The governing equations are first formulated in the coordinate system (ξ, y, z, t) attached to the moving heat source. To treat the convective velocity as the primary unknown in the governing equations, the equations are further modified by subdividing the net velocity into convective and welding velocity components as follows:

$$\mathbf{V}' = \mathbf{V} + \mathbf{U} \tag{1}$$

Here $\mathbf{V}'$ is the net velocity at any point with respect to the frame attached to the heat source, $\mathbf{V}$ is the convective component of the velocity, and $\mathbf{U}$ is the welding velocity. Using the relation in Eq. (1), the steady state versions of the modified governing equations can be derived with $\mathbf{V}$ as the primary unknown velocity. The details of the derivation are given in the appendix. The final forms of the equations are given below.

Continuity

$$\nabla \cdot (\rho \mathbf{V}) = 0 \tag{2}$$

where ρ is the density.

Momentum

$$\nabla \cdot (\rho \mathbf{V}\mathbf{V}) = -\nabla P + \nabla \cdot (\mu \nabla \mathbf{V}) + S_{c\text{-}p} + S_b - \nabla \cdot (\rho \mathbf{U}\mathbf{V}) \tag{3}$$

Here μ is the viscosity, P is effective pressure, $S_{e\text{-}p}$ represents the source term that modifies the momentum equation in the mushy zone, and S_b is the source term that takes into account the buoyancy force in the weld pool. The last term in Eq. (3) arises due to the motion of the heat source.

The Bousinesq approximation is used to treat the buoyancy force. Thus the density is assumed to be constant in all terms except the buoyancy force term. Furthermore, the buoyancy force is taken into account by assuming the density to vary linearly with temperature. After coupling the hydrostatic pressure with the static pressure, the buoyancy source term S_b is given by

$$S_b = \rho g \beta (T - T_{ref}) \tag{4}$$

where β is the thermal expansion coefficient and T_{ref} is any arbitrarily selected reference temperature.

The effective tangential stress τ due to the Marangoni stress on the free surface is calculated as follows:

$$\tau = f_l \frac{d\gamma}{dT} \nabla T \tag{5}$$

where $d\gamma/dT$ is the temperature coefficient of surface tension and f_l is the liquid fraction, which is assumed to vary linearly with temperature in the mushy region. The fraction f_l takes into account the decrease in the shear stress in the mushy region.

The Carman-Koseny equation [11] is used to define the source term $S_{e\text{-}p}$ in the mushy region. The equation is derived from Darcy's law and is given by

$$S_{e\text{-}p} = -A(f_l)\mathbf{V}_i \tag{6}$$

where A is determined according to the Carman-Kozeny equation [11] for flow through porous media as follows:

$$A = -C\left(\frac{1 - f_l^2}{f_l^3 + B}\right) \tag{7}$$

where B is a very small positive number introduced to avoid division by zero. By choosing a large value of C, this source term forces the velocity in the solid region ($f_l = 0$) to be zero.

Energy Equation

The technique used here to account for the phase change is based on the works of Voller and Prakash [10] and Brent et al. [11]. The total enthalpy of the material H is represented as a sum of sensible heat, $h = \int C_p \, dT$, and latent heat content ΔH, i.e.,

$$H = h + \Delta H \tag{8}$$

The latent heat content, $\Delta H = F(T)$, is assumed to vary linearly with temperature, i.e.,

$$F(T) = L \qquad T > T_l$$

$$F(T) = L\left(\frac{T - T_s}{T_l - T_s}\right) \qquad T_s \le T \le T_l \tag{9}$$

$$F(T) = 0 \qquad T < T_l$$

where L is the latent heat, T_l is the liquidus temperature, and T_s is the solidus temperature. The liquid fraction f_l is also calculated from a relationship similar to the one presented in Eq. (9).

The modified energy equation is given by

$$\nabla \cdot (\rho \mathbf{V} h) = \nabla \cdot \left(\frac{k}{C_p} \nabla h\right) + S_l - \nabla \cdot (\rho \mathbf{U} h) \tag{10}$$

where C_p is the specific heat, k is the thermal conductivity, and S_l is the source term that accounts for latent heat of melting and convective transport of latent heat in the two-phase region (mushy zone). The source term S_l is given by

$$S_l = -[\nabla \cdot (\rho \mathbf{V} \Delta H) + \nabla \cdot (\rho \mathbf{U} \Delta H)] \tag{11}$$

The last term in Eq. (10) accounts for the transport of sensible enthalpy due to the motion of the heat source. Similarly, the last term in Eq. (11) represents the latent heat exchange due to the phase change occurring at the pool boundaries due to the movement of the heat source.

COMPUTATIONAL METHOD AND DETAILS

The control-volume-based computational method of Patankar [12], implemented in COMPACT-3D [13], is used for the numerical solution of the governing equations. A brief summary of the method is provided below.

The computational domain is divided into control volumes. A main grid point is located at the center of each control volume. The values of scalar variables such as pressure and enthalpy are stored at the main grid points. A staggered grid is used to store the velocity components. Thus the momentum control volumes are staggered with respect to the main control volumes. Typical control volumes for a scalar variable and for a momentum equation in the ξ direction are given in Figure 2. Discretization equations for a particular varible are formulated by integrating the corresponding conservation equation over the respective control volumes. The combined convective-diffusive fluxes over the faces of the control volumes are computed using the power law scheme [12].

It is of interest to discuss the discretization of the additional source terms in the modified governing equations. The source terms are of the convective form, and their discretization is illustrated for the energy equation. The source term

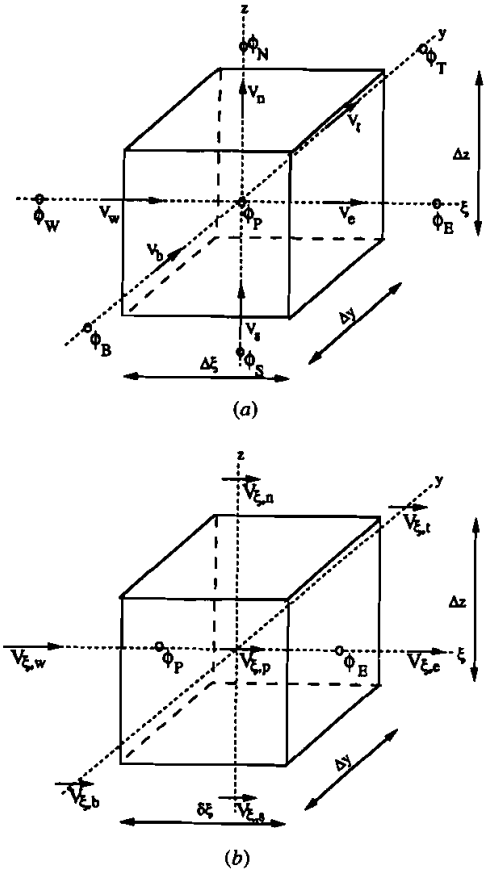

Figure 2. Control volumes for (*a*) the enthalpy equation and (*b*) the momentum equation in the ξ direction.

$-\nabla \cdot (\rho \mathbf{V} \Delta H)$ in Eq. (11), using Figure 2*a* and the upwind scheme, can be discretized as follows:

$$\begin{aligned} S_l = -\nabla \cdot (\rho \mathbf{V} \Delta H) = {} & [[0, F_w]] \Delta H_W - [[0, -F_w]] \Delta H_P + [[0, -F_e]] \Delta H_E \\ & - [[0, F_e]] \Delta H_P + [[0, F_s]] \Delta H_S - [[0, -F_s]] \Delta H_P \\ & + [[0, -F_n]] \Delta H_N - [[0, F_n]] \Delta H_P + [[0, F_b]] \Delta H_B \\ & - [[0, -F_b]] \Delta H_P + [[0, -F_t]] \Delta H_T - [[0, F_t]] \Delta H_P \end{aligned} \tag{12}$$

where $[[p, q]]$ means the maximum of p and q and F denote the flow rates through the faces of the control volume. Thus the flow rate for the west face F_w is given by

$$F_w = \rho V_\xi \, \Delta y \, \Delta z \tag{13}$$

Similarly, the source term $-\nabla \cdot (\rho \mathbf{U} \Delta H)$ in Eq. (11) is discretized as follows:

$$-\nabla \cdot (\rho \mathbf{U} \Delta H) = [[0, F]] \Delta H_W - [[0, -F]] \Delta H_P + [[0, -F]] \Delta H_E - [[0, F]] \Delta H_P \quad (14)$$

where $F = \rho U_\xi \Delta y \Delta z$. The terms in the y and z direction do not appear in Eq. (14). This is due to the fact that the welding velocity U is assumed to be in the ξ direction only.

The last term in Eq. (10), $-\nabla \cdot (\rho \mathbf{U} h)$, arises due to the motion of the heat source and is discretized in a manner identical to Eq. (14). The same treatment is used for discretizing the source term in the momentum equations, $-\nabla \cdot (\rho \mathbf{U} \mathbf{V})$, which arises due to the motion of the heat source. Appropriate changes in the coefficients of the discretized momentum and energy equations are made to incorporate the discretized source terms.

The velocity-pressure coupling in the discretized momentum equations is handled using the SIMPLER algorithm [12]. For each variable, the solution of the discretized equations is achieved by using a line-by-line method coupled with a block-correction scheme [13].

The numerical methodology has been applied to a three-dimensional laser welding problem. The symmetry of the physical situation is exploited to limit the computational domain to half of the block to save computational effort. The plane of symmetry corresponds to the $y = 0$ plane. The length of the block in the ξ direction is sufficiently long that any further increase in the length does not affect the solution in the region of interest in any appreciable fashion. The domain is discretized using a grid size of $69 \times 35 \times 32$. Spatially nonuniform grids are used for maximum resolution. The grids are finer near the heat source in all three directions. In the z direction, very fine grids are used near the surface to give an accurate representation of Marangoni stress. The minimum grid size was 0.00032 cm.

The prescription of the heat exchange between the heat source and the surface of the sample was given by a Gaussian distribution:

$$\mathbf{J}_h(\xi, y, z)_{z=0} = \frac{3Q\eta}{\pi r_b^2} \exp\left(-\frac{3(\xi^2 + y^2)}{r_b^2}\right) \quad (15)$$

where Q is the power input, η is the welding process efficiency, and r_b is the beam radius. The values of these parameters are listed in Table 1. At the plane of symmetry, the gradient of enthalpy, dh/dy, is zero. At other surfaces the enthalpy of the material is taken as the enthalpy corresponding to the room temperature, since the computational domain is taken to be sufficiently large compared with the size of the weld pool. At the plane of symmetry, V_y and the normal gradients of V_ξ and V_z are taken as zero. The top surface is assumed to be flat and subject to shear stress due to Marangoni force. Also V_z is defined to be zero at the surface.

RESULTS

The steady state three-dimensional temperature fields obtained from the solution of the governing equations are shown in Figures 3*a* and 3*b* for the two welding velocities (0.0027 and 0.0014 m/s). For clarity, only the section of the computational domain just below the heat source is shown in the figure. As expected, the pool size for the low-velocity case is larger than that for the high-velocity case. Also the peak temperature for the high-velocity case is lower than that for the low-velocity case. The temperature fields show typical elongated pool shapes for both cases. The pool length to width ratio is greater for the high-velocity case (1.23) compared with the low-velocity case (1.15). This is expected with the limiting case being zero welding velocity, which would result in pools of equal length and width under most welding conditions. Also, the tempera-

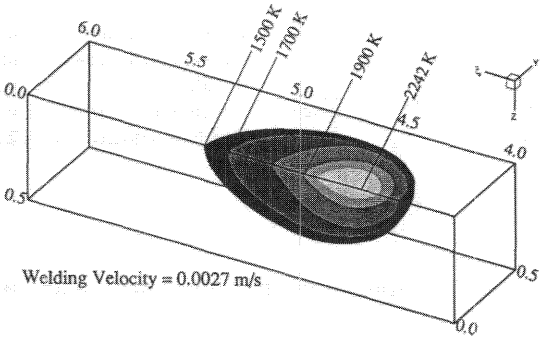

(*a*)

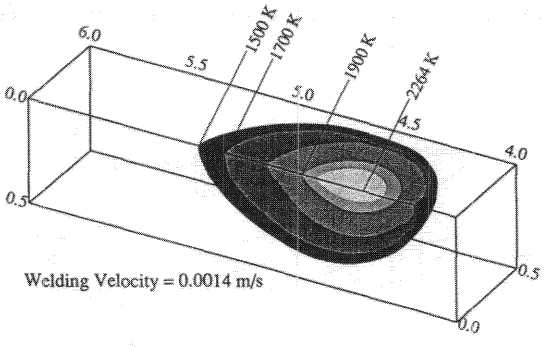

(*b*)

Figure 3. Calculated three-dimensional temperature distributions for (*a*) the welding conditions given in Table 1 and welding velocity of 0.0027 m/s and (*b*) the welding conditions given in Table 1 and welding velocity of 0.0014 m/s. The dimensions are in centimeters.

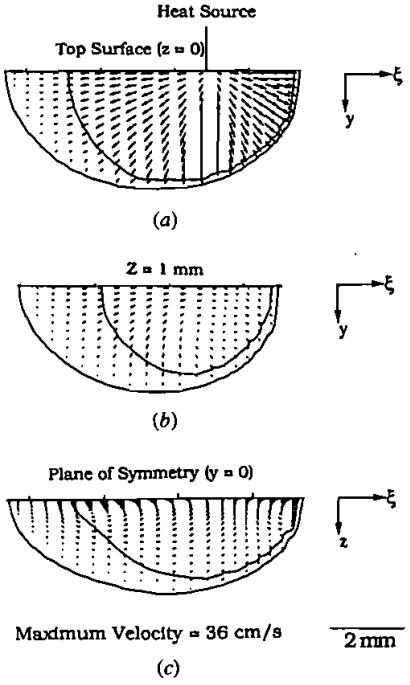

Figure 4. Calculated velocity fields (*a*) on the weld pool surface, (*b*) at $z = 1$ mm, and (*c*) along the plane of symmetry for the welding conditions given in Table 1. Welding velocity is 0.0027 m/s.

ture gradients are greater in front of the moving heat source than behind the heat source.

The velocity fields in the molten pool on three cross sections of the computational domain are shown in Figure 4 for the high welding velocity. These cross sections of the computational domain are shown in Figure 5. Velocities in Figure

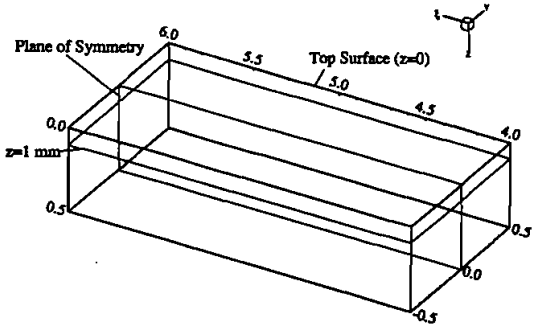

Figure 5. Different cross sections of the computational domain where velocity fields are presented. The dimensions are in centimeters.

4*a* show that at the weld pool surface, the liquid metal moves from the middle, where the temperature is high, toward the periphery of the weld pool, where the metal has a relatively low temperature. This is expected for a metal with a very low concentration of surface active elements, which will result in a negative temperature coefficient of surface tension, $d\gamma/dT$, over much of the weld pool surface. In the calculation, a constant negative $d\gamma/dT$ was assumed. The strong outward flow at the pool surface results an inward flow within the weld pool. This is observed from Figure 4*b*. The flow field on the plane of symmetry is show in Figure 4*c*. The flow is radially outward on the surface, which is consistent with the flow pattern shown in Figure 4*a*. A short distance below the surface the flow becomes inward, both in front of and behind the heat source.

The velocity fields for the low welding velocity case are shown in Figure 6 on the same cross sections of the computational domain as for the high-velocity case. The general features of the velocity field are similar to the velocity fields for the high welding velocity case. However, the maximum velocity on the pool surface for the low welding velocity is slightly lower than that for the high welding velocity. This is expected because of reduced temperature gradients on the pool surface due

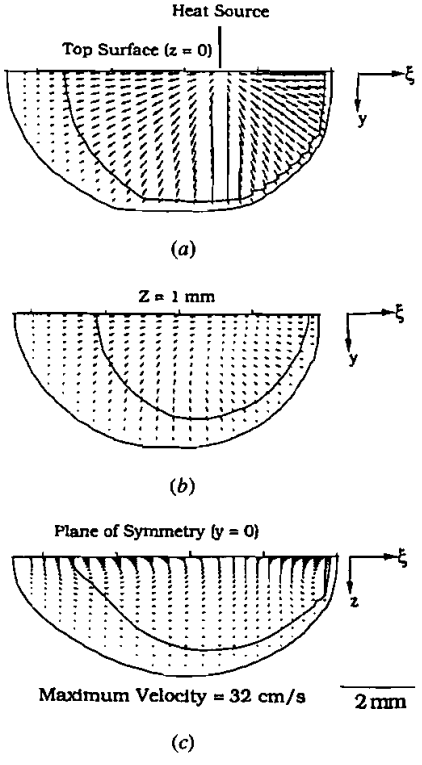

Figure 6. Calculated velocity fields (*a*) on the weld pool surface, (*b*) at $z = 1$ mm, and (*c*) along the plane of symmetry for the welding conditions given in Table 1. Welding velocity is 0.0014 m/s.

to greater pool size. As a consequence, the Marangoni stress is slightly reduced, resulting in lower velocity. Comparison of the pool geometry in Figures 4 and 6 clearly shows the larger pool size for the low welding velocity case. It is also observed from Figures 4 and 6 that the length of the mushy zone is much greater behind the heat source than in front of the heat source. Furthermore, the intensity of the flow in the mushy zone decreases as the liquid-solid interface is reached. This is due to the increased resistance to flow in the mushy zone because of the increase in the source term [Eq. (7)]. The flow in the mushy zone can have important consequences on the microstructure of the weldment by influencing the extent of solute segregation and also the solidification structures.

The temperature-time data at different locations in the weld metal play an important role in determining weld metal microstructure and properties. From the steady state temperature field, obtained from the solution of the transformed momentum and enthalpy equation, temperature as a function of time at different locations (x, y, z) can be calculated by the following relation:

$$T(x, y, z, t_2) = \frac{T(\xi_2, y, z) - T(\xi_1, y, z)}{\xi_2 - \xi_1} U(t_2 - t_1) + T(x, y, z, t_1) \quad (16)$$

where $T(\xi_2, y, z)$ and $T(\xi_1, y, z)$ are the steady state temperatures at coordinates (ξ_2, y, z) and (ξ_1, y, z), respectively; $(\xi_2 - \xi_1)$ is the distance traveled by the beam in time $(t_2 - t_1)$; and $T(x, y, z, t_1)$ and $T(x, y, z, t_2)$ are the temperatures at location (x, y, z) at times t_1 and t_2, respectively. The temperature-time data at any monitoring location at the top surface of the weld centerline $(x > 0, y = 0, z = 0)$ obtained from Eq. (16) are presented in Figure 7 for the two welding velocities, 0.14 and 0.27 cm/s. All the points on the weld centerline will experience the same thermal history. The results in Figure 7 show that lower welding velocity results in lower heating and cooling rates. The cooling rates obtained from the numerical modeling results can be used to predict weld metal microstructure and, eventually, properties [14].

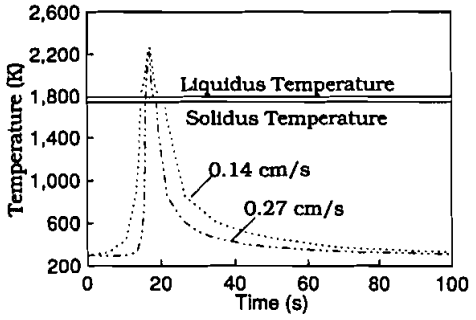

Figure 7. Calculated temperature-time data at the weld centerline ($y = 0$ and $z = 0$) for two cases.

SUMMARY

A method is presented for improved computational analysis of heat transfer and fluid flow during welding with a moving heat source. The governing equations are formulated in the reference frame attached to the moving heat source. The equations are further modified to treat the physical velocity of the liquid metal relative to the specimen as the primary unknown velocity. This modification results in physically meaningful source terms that contain the effect of the moving source term in the governing equations. A control-volume-based computational method is used for the solution of the governing equations. The numerical results of the methodology are presented in the form of temperature and flow fields and temperature-time data for two welding velocities. The effect of the welding velocity on the temperature and flow fields and the temperature-time data illustrates the utility of the computational analysis for welding practice.

REFERENCES

1. S. A. David and T. DebRoy, Current Issues and Problems in Welding Science, *Science*, vol. 257, pp. 497–502, 1992.
2. T. DebRoy and S. A. David, Physical Processes in Fusion Welding, *Rev. Mod. Phys.*, vol. 67, pp. 85–112, 1995.
3. S. Kou and D. K. Sun, Fluid Flow and Weld Penetration in Stationary Arc Welds, *Metall. Trans. A*, vol. 16A, pp. 203–213, 1985.
4. T. Zacharia, S. A. David, J. M. Vitek, and T. DebRoy, Weld Pool Development During GTA and Laser Beam Welding of Type 304 Stainless Steel, Part 1: Theoretical Analysis, *Welding J. Res. Suppl.* vol. 68, no. 12, pp. 499–509, 1989.
5. A. Paul and T. DebRoy, Free Surface Flow and Heat Transfer in Conduction Mode Laser Welding, *Metall. Trans. B*, vol. 19B, pp. 851–858, 1988.
6. T. Zacharia, S. A. David, J. M. Vitek, and T. DebRoy, Modeling of Interfacial Phenomena in Welding, *Metall. Trans. B*, vol. 21B, pp. 600–603, 1990.
7. C. Chan, J. Mazumder, and M. M. Chen, A Two-Dimensional Transient Model for Convection in Laser Melted Pool, *Metall. Trans. A*, vol. 15A, pp. 2175–2184, 1984.
8. S. Kou and Y. H. Wang, Three-Dimensional Convection in Laser Melted Pools, *Metall. Trans. A*, vol. 17A, pp. 2265–2270, 1986.
9. C. Prakash, M. Sammonds, and A. K. Singhal, A Fixed Grid Numerical Methodology for Phase Change Problems Involving a Heat Source, *Int. J. Heat Mass Transfer*, vol. 30, no. 12, pp. 2690–2694, 1987.
10. V. R. Voller and C. Prakash, A Fixed Grid Numerical Methodology for Convection-Diffusion Mushy Region Phase-Change Problems, *Int. J. Heat Mass Transfer*, vol. 30, no. 8, pp. 1709–1719, 1987.
11. A. D. Brent, V. R. Voller, and K. J. Reid, Enthalpy-Porosity Technique for Modeling Convection-Diffusion Phase Change: Application to the Melting of a Pure Metal, *Numer. Heat Transfer*, vol. 13, pp. 297–318, 1988.
12. S. V. Patankar, *Numerical Heat Transfer and Fluid Flow*, Hemisphere, New York, 1980.
13. Innovative Research, Inc., Documentation of COMPACT-3D Version 3.1, Minneapolis, Minnesota, 1994.
14. K. Mundra, T. DebRoy, S. Babu, and S. A. David, Weld Metal Microstructure Calculations from Fundamentals of Transport Phenomena in the Arc Welding of Low Alloy Steels, *Welding Journal* (submitted).

APPENDIX

Momentum Equation in Moving Coordinate System (ξ, y, z)

The momentum equation in the ξ, y, z coordinate system is given by

$$\nabla \cdot (\rho \mathbf{V}'\mathbf{V}') = -\nabla P + \mu \mathbf{V} \cdot (\nabla \mathbf{V}') + S \tag{A1}$$

The first term on the left-hand side of Eq. (A1), for constant material density, can be simplified as follows:

$$\begin{aligned}\nabla \cdot \rho \mathbf{V}'\mathbf{V}' = {} & \rho\left(V_\xi' \frac{\partial V_\xi'}{\partial \xi} + V_y' \frac{\partial V_\xi'}{\partial y} + V_z' \frac{\partial V_\xi'}{\partial z}\right)\mathbf{i} \\ & + \rho\left(V_\xi' \frac{\partial V_y'}{\partial \xi} + V_y' \frac{\partial V_y'}{\partial y} + V_z' \frac{\partial V_y'}{\partial z}\right)\mathbf{j} \\ & + \rho\left(V_\xi' \frac{\partial V_z'}{\partial \xi} + V_y' \frac{\partial V_z'}{\partial y} + V_z' \frac{\partial V_z'}{\partial z}\right)\mathbf{k}\end{aligned} \tag{A2}$$

Substituting, from Eq. (A2), $V_\xi' = V_\xi + U_\xi$, $V_y = V_y + U_y$, and $V_z = V_z + U_z$, and realizing that derivatives of scanning velocity components with respect to ξ or y or z will be zero, we have

$$\begin{aligned}\nabla \cdot \rho \mathbf{V}'\mathbf{V}' = {} & \rho\left(V_\xi \frac{\partial V_x}{\partial \xi} + V_y \frac{\partial V_\xi}{\partial y} + V_z \frac{\partial V_\xi}{\partial z}\right)\mathbf{i} \\ & + \rho\left(U_\xi \frac{\partial V_\xi}{\partial \xi} + U_y \frac{\partial V_\xi}{\partial y} + U_z \frac{\partial V_\xi}{\partial z}\right)\mathbf{j} + \cdots\end{aligned} \tag{A3}$$

Writing in vector form, we have

$$\nabla \cdot (\rho \mathbf{V}'\mathbf{V}') = \nabla \cdot (\rho \mathbf{V}\mathbf{V}) + \nabla \cdot (\rho \mathbf{U}\mathbf{V}) \tag{A4}$$

From Eq. (A2), the second term on the right can be simplified as follows:

$$\nabla \cdot (\nabla \mathbf{V}') = \nabla \cdot [\nabla(\mathbf{V} + \mathbf{U})] \tag{A5}$$

Since the scanning velocity is constant, we have $\nabla \mathbf{U} = 0$. Substituting this relation in Eq. (A5), we have

$$\nabla \cdot (\nabla \mathbf{V}') = \nabla \cdot (\nabla \mathbf{V}) \tag{A6}$$

Substituting Eq. (A4) and (A6) into Eq. (A1) results in the following modified equation:

$$\nabla \cdot (\rho \mathbf{V}\mathbf{V}) = -\nabla P + \mu \nabla \cdot (\nabla \mathbf{V}) + S - \nabla \cdot (\rho \mathbf{U}\mathbf{V})$$

Energy Equation in Moving Coordinate System (ξ, y, z)

The energy equation in a moving coordinate system is given by [9]

$$\nabla \cdot (\rho \mathbf{V}' h) = \nabla \cdot \left(\frac{\mathbf{k}}{C_p} \nabla h \right) + S_1 \tag{A7}$$

where S_1 is given by [9]

$$S_1 = -\nabla \cdot (\rho \mathbf{V}' \Delta H) \tag{A8}$$

Substituting Eq. (A2) into Eqs. (A7) and (A8) results in the modified energy equations, Eqs. (10) and (11).